An Improved Gray Wolf Optimizer MPPT Algorithm for PV System With BFBIC Converter Under Partial Shading

KE GUO[1], LICHUANG CUI[1], MINGXUAN MAO[1,2], (Member, IEEE), LIN ZHOU[1], AND QIANJIN ZHANG[1]

[1]State Key Laboratory of Power Transmission Equipment and System Security and New Technology, School of Electrical Engineering, Chongqing University, Chongqing 400044, China
[2]Postdoctoral Station of Electrical Engineering, Chongqing University, Chongqing 400044, China

Corresponding author: Mingxuan Mao (mx_m@cqu.edu.cn)

ABSTRACT Based on the boost full bridge isolated converter (BFBIC) topology and considering the sudden changes in the external environment, a global maximum power point tracking (GMPPT) control strategy based on an improved gray wolf optimizer (IGWO) algorithm is proposed in this paper. In the strategy, a nonlinear tangent trigonometric function as a convergence factor is integrated into the gray wolf optimizer (GWO) algorithm. In addition, the active-clamp circuit and phase-shift are used to implement the soft switch technology for BFBIC converter in photovoltage (PV) system. Finally, the maximum power point tracking (MPPT) performance on PV system with the proposed IGWO algorithm under static and dynamic partial shading conditions (PSCs) was investigated and compared with other common perturb and observe(P&O), particle swarm optimization (PSO), artificial bee colony (ABC), adapt inertia weight salp swarm algorithm (WSSA), salp swarm algorithm with grey wolf optimizer (SSA-GWO), SSA with PSO (SSA-PSO), enhanced GWO (EGWO) MPPT algorithms. The effectiveness and stability of the proposed control strategy are validated, especially tracking speed under PSCs. Simulation results show that the BFBIC topology with the proposed IGWO algorithm outperforms other algorithms on most cases, especially only takes the tracking time of 0.24s and reaches the efficiency of 98.54% under the most severe PSCs.

INDEX TERMS Boost full bridge isolated converter (BFBIC), improved grey wolf optimizer (IGWO), global maximum power point tracking (GMPPT), partial shading conditions (PSCs).

I. INTRODUCTION

Harmonic resonances and reactive power transmission issues of Alternating Current (AC) booster and gathering system are gradually exposed with the increasing scale of distributed photovoltage (PV) power plants. Due to this issue, not only the safety and stability capability of the PV power plants and the power system will be affected severely, but also the transmission capability of the PV power plants can be also constrained. By contrast, Direct Current (DC) booster gathering system does not have the inherent stability issues, such

as power angle stability, harmonic resonances, the voltage stability and power quality problems caused by the excess or lack of reactive power. Therefore, to solve the above issue., the DC booster gathering system will be the future development direction of PV power plants [1]–[4].

Due to the low voltage and DC output characteristics of PV arrays, one of the main bottlenecks of the DC booster gathering technology is the key topologies [5], such as high power or high voltage DC-DC converters. Theoretically, a basic boost converter can provide infinite voltage gain with an extremely high duty ratio. In practice, the voltage gain is limited by the parasitic components, inductance, and capacitance, and cannot reach the theoretical value. On the other hand, because

---

The associate editor coordinating the review of this manuscript and approving it for publication was Jenny Mahoney.

of the small input voltage, the input current is usually large in high power and high voltage conversion. This feature makes it difficult to choose the main switches and diodes [6]. Currently, the topologies are widely applicable to high-power and high-voltage applications mainly including resonant circuits [7], [8] and modular multilevel [9], [10]. Although the resonant circuit is small and lightweight, the control is extremely complicated and the parameter of resonant inductance and capacitance are difficult to determine. The modular multilevel converter (MMC) has been employed in the DC system represented by the high voltage direct current (HVDC) power transmission [11]. It has a highly modular structure and high reliability, but it was only applied to AC-DC converters.

Many different converter topologies have been found, where the boost full bridge isolated converter (BFBIC) often concerned by research scholars [12]–[15]. Watson and Lee proposed BFBIC with an active-clamp circuit to achieve zero-voltage switching operation and to reduce the voltage stress on the power switches [16]. Reference [17] proposed an BFBIC which features wide input range and resilient operation along 0 to 100 percent of load current change with a set of active voltage clamping snubber and active start-up circuits, avoid the start-up problem caused by the low output capacitor voltage at the beginning of start-up, the leakage inductance of the isolation transformer. To achieve the purpose of regulating control of the output voltage under varying load, the literature [18] deals with the achievement of the dynamic response of high gain DC-DC converter in PV system using BAT Algorithm optimization tuned fuzzy sliding mode controller. The dynamic and transient response of the isolated full bridge DC-DC converter are improved under starting and load step change conditions. In [19], a new two-input isolated boost DC-DC converter based on a distributed multi-transformer structure, which is suitable for hybrid renewable energy systems is investigated and designed. the two-input ports can be decoupled completely, so the converter can draw the power from the two different DC sources, which have low output voltage, and transfer it to the DC bus, which has high voltage, separately or simultaneously. A new soft-switching snubberless naturally clamped method is proposed in the paper [20]. Zero-current commutation of current-fed devices makes the converter snubberless and fully soft-switched with natural clamping of the devices' voltage. However, it still cannot solve the high voltage and current stress on the devices.

The BFBIC topology has several merits such as two-way magnetization, high power, input and output isolation. But its major disadvantage is that start-up problem, leakage inductance problem of isolated transformer and magnetic reset problem of input induct. Despite proposed various improve method to avoid some disadvantage, it does not combine the common problems of PV power generation systems when applied to the PV DC booster gathering system, that is, the mutation of the external environment causes the distributed PV arrays to operate under partial shading conditions (PSCs) [21], [22]. If the traditional maximum power point tracking (MPPT) methods, such as perturb and observe

(P&O), increment conductance (INC), etc., are adopted under PSCs, the PV system will be easy to fall into the local maximum power point (LMPP), which will reduce its efficiency. A control strategy for BFBIC circuit is proposed in [21], in which P&O is used by MPPT and the compensators of the voltage controller is adopted. However, the method is only suitable for uniform irradiation.

These algorithms have better performance under PSCs, such as particle swarm optimization (PSO) [23], salp swarm algorithm (SSA) [24], whale optimization algorithm (GOA) [25], shuffled frog leaping algorithm (SFLA) [26], etc.. In [27], a modified particle velocity-based PSO algorithm is proposed by modified the speed update formula of the conventional PSO algorithm, namely, adaptive weighting factor and adaptive cognitive acceleration constant are adopted. The algorithm eliminates the inherent randomness of conventional algorithms and relatively improves the response speed, tracking speed and accuracy under frequent or progressive irradiation changes. A GOA algorithm is proposed in [25] to eliminates the computational burden and reduces the power oscillation during the change in operating conditions. In [28]–[30], an algorithm combining artificial bee colony algorithm (ABC), ant colony algorithm (ACO), PSO algorithm and P&O method is proposed respectively, which combines the global search ability of intelligent algorithms with the local search ability of P&O method, and use the MPPT control under PSCs. The GWO algorithm is used in PV generation system for the first time in [31]. The MPPT controller is achieved by combining SSA with GWO [32]. The leader structure of the GWO algorithm is introduced into the basic SSA algorithm to enhance the global search capability. Davoodkhani *et al.* [36] proposes to use the optimal duty ratio determined by GWO as the initial value of crow search algorithm (CSA) for MPPT. In addition to the about GWO hybrid method, the method of calculating the DC impedance of PV string by GWO to indirectly carry out MPPT is proposed to avoid the local extreme problems [37]. Enhanced GWO (EGWO) [38] was proposed by simplifying the calculation process, this method is directly used for PV generation system to track the global maximum power point tracking (GMPPT) of PV system under PSCs with high accuracy and short tracking time, therefore EGWO will be used to compared with the method proposed in this paper.

In this paper, a novel nature-inspired IGWO MPPT method is proposed to apply for BFBIC topology to further improve the response speed, system stability, better adapt to changes in the external environment. In the proposed strategy, a nonlinear tangent trigonometric function as a convergence factor is integrated into the GWO algorithm. Moreover, the active-clamp circuit and phase-shift are used to implement the soft switch technology for BFBIC converter in PV system. The Markov process and convergence in probability are adopted to evaluate the convergence of IGWO algorithm. Finally, the proposed method was simulated in a BFBIC topology under static and dynamic conditions and compared with conventional P&O, PSO, ABC, WSSA, SSA-PSO, SSA-GWO,
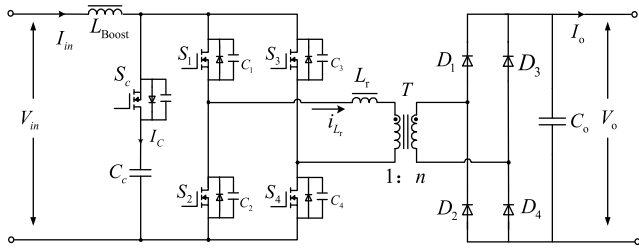
FIGURE 1. The topology structure of BFBIC with active clamp.

EGWO algorithm to validate the rapidity of this novel MPPT method.

The remainder of the paper is organized as follows. The topology structure of BFBIC and the proposed control strategy are elaborated on in Section 2 and Section 3, respectively. The Section 4 analysis convergence of the IGWO algorithm. The simulations in Section 5 give a comprehensive comparison for the performance of IGWO algorithm and the other algorithm under static and dynamic PSCs. Finally, the conclusions are given in Section 6.

II. THE TOPOLOGY STRUCTURE OF THE BFBIC CONVERTER

Considering that the PV DC booster gathering system requires a high power, high ratio converter, in this paper, the BFBIC is adopted as the converter topology to realize MPPT and DC booster control of the PV arrays. The topology structure is shown in Fig.1. In Fig.1, L_{Boost} is the boost inductor; switches S_1-S_4 together form a full-bridge circuit, C_{s1}- C_{s4} are the junction capacitance of the switches; L_r is the equivalent leakage inductance of the transformer; C_0 is the output capacitor; S_c and C_c constitute an active-clamp circuit for controlling the peak voltage at both end of switches caused by leakage inductance of transformer, realizing zero-voltage switching (ZVS), and reducing the voltage stress of the switches.

Fig.2 shows the timing diagram and the key waveforms of the converter. The phase difference of the driving pulse of S_1, S_4 is 180° different form that of S_2, S_3. The duty cycle range is (0.5,1) during normal operation. This is because the energy of the inductor L_{Boost} has no release the loop when the switches S_1-S_4 are turned off simultaneously, resulting in a large peak voltage at both ends of the switches.

Stage1 ($<t_1$): all four switches S_1-S_4 are turned on, and the circuit operates in boost mode. In addition, the inductor current increases linearly at a slope of V_{in}/L_{Boost}. The output voltage is provided by the output capacitor C_0.

Stage 2 (t_1- t_2): the switches S_2, S_3 are turned off. At this time, the active clamp switch S_c is still turned off. Partial inductor current is transferred to the clamp capacitor C_c through the body diode of S_c. It is possible to suppress peak voltage caused by the presence of leakage inductance.

Stage 3 (t_2- t_4): at t_2, due to the presence and conduction of the body diode of the active clamp switch S_c, the voltage at both ends of the switch S_c is approximately zero. the S_c is turned on with ZVS. The energy stored in the inductor current
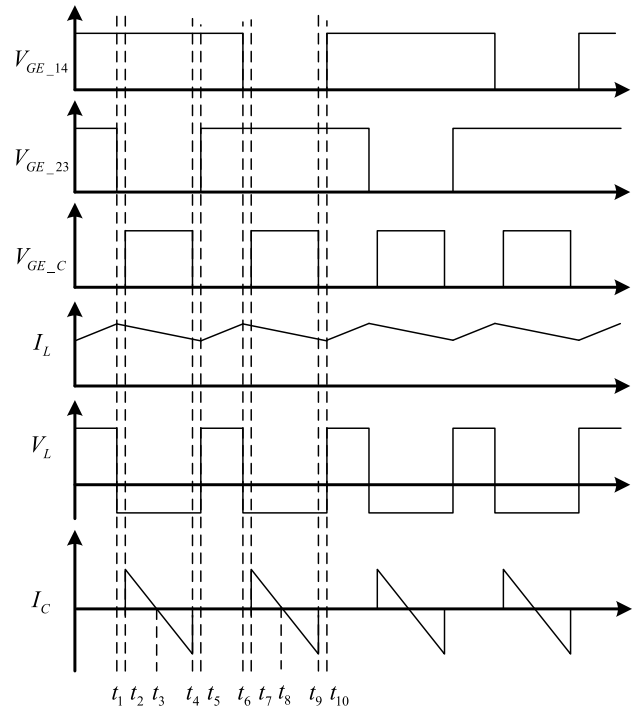

FIGURE 2. The timing diagram and the key waveforms of the converter.

and the clamp capacitor is output to the load. At this time, the leakage current of the transformer is greater than the input inductor current.

Stage 4 (t_4- t_5): at t_4, the active clamp switch S_c is turned off. Owing to the leakage current of the transformer is greater than the input inductor current, the excess current flows to the junction capacitance of S_2 and S_3, and the junction capacitance charge. The body diode of S_2, S_3 is turned on when leakage current of the transformer is equal to the input inductor current

Stage 5 (t_5- t_6): the body diode is turned on to achieve ZVS of the switches S_2, S_3. Hence, the circuit will operate at the Boost mode since the switches S_1-S_4 are turned on simultaneously.

After t_6, the circuit enters the second half of the cycle, and operates like Stage 1 - Stage 5.

It can be seen from Fig.2 that the inductor current fluctuates twice and the amount of current increase is equal to the amount of decrease in one cycle. Therefore, the inductor energy is balanced. When the switches S_1-S_4 are turned on simultaneously, Inductor L_{Boost} is charged by the input voltage V_{in}, inductor current increases linearly at a slope of V_{in}/L_{Boost}. The input voltage is expressed as:

$$V_{in} = L\frac{di_{L_{Boost}}}{dt} \quad (1)$$

When the switches S_1, S_4 or the switches S_2, S_3 are turned on, V_{in} and L_{Boost} will releases energy to the secondary side through the isolation transformer, causing the inductor current to decrease:

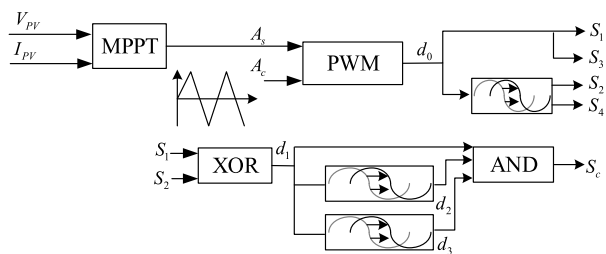$$V_{in} - \frac{V_0}{n_T} = L\frac{di_{L_{Boost}}}{dt} \quad (2)$$

FIGURE 3. The basic control flow chart.

Hence, based on the principle of volt-second balance, the input and output relationship of the circuit can be obtained, as follow:

$$V_0 = \frac{n_T V_{in}}{2(1-D)} \quad (3)$$

where n_T is ratio of the isolation transformer.

III. THE IGWO MPPT CONTROL STRATEGY OF THE BFBIC CONVERTER

In the PV DC booster gathering system, the BFBIC topology is used to achieve high voltage output. The basic control flow chart is shown in Fig.3. The control scheme samples V_{PV} and I_{PV} from the PV arrays and produces duty signal of switches S_1-S_4. The MPPT controller generates the carrier of the pulse width modulation (PWM) by processing the V_{PV} and I_{PV}. The PWM generator generates the duty signal d_0. The signal d_0 acts directly on the switches S_1, S_3 or through a phase-shift namely delayed by half a cycle, producing signals for the switches S_2, S_4. Similarly, the duty signal of the active clamp switch S_C is obtained by Exclusive OR (XOR) of the switches S_1, S_2. The ZVS of the active clamp switch S_C and the switch S_1-S_4 is realized by the AND gate of the duty signal d_1, d_2, d_3. Through the use of phase-shift, the control of the active-clamp circuit is realized, and the major disadvantage of the BFBIC converter are eliminated, such as start-up problem, leakage inductance problem.

A. THE DESCRIPTION OF GWO

The GWO algorithm was proposed by Mirjalili *et al.* in 2014 based on hunting technique and the social hierarchy of grey wolves [33]. According to the gray wolf population hierarchy, the wolves are divided into four categories: alpha (α), bate(β), delta(δ), omega(w). In the practical application of the GWO algorithm, we consider the fittest solution as the α. The second and third best solutions are selected β and δ respectively. The rest of the candidate solutions are assumed to be w. To update the position of the grey wolves the following equations are proposed [32]:

$$\vec{D} = \left| \vec{C} \cdot \vec{X}_P(t) - \vec{X}(t) \right| \quad (4)$$

$$\vec{X}(t+1) = \vec{X}_p(t) - \vec{A} \cdot \vec{D} \quad (5)$$

where t is the current iteration, $\vec{X}_P$ is the position of the prey, $\vec{X}$ is the position of the grey wolf, $\vec{A}$, $\vec{C}$ and $\vec{D}$ are

coefficient vectors. The vectors $\vec{A}$ and $\vec{C}$ are calculated as follow [33]:

$$\vec{A} = 2\vec{a} \cdot \vec{r}_1 - \vec{a} \quad (6)$$

$$\vec{C} = 2 \cdot \vec{r}_2 \quad (7)$$

where r_1, r_2 are random vectors in [0, 1] and a decrease linearly from 2 to 0.

The hunting (optimization) is usually guided by the α. the β and δ might also participate in the hunting occasionally. The w wolves follow these three wolves. The position update formula is as follows [33]:

$$\vec{D}_\alpha = \left| \vec{C}_1 \cdot \vec{X}_\alpha(t) - \vec{X}(t) \right|, \quad \vec{D}_\beta = \left| \vec{C}_2 \cdot \vec{X}_\beta(t) - \vec{X}(t) \right|,$$
$$\vec{D}_\delta = \left| \vec{C}_3 \cdot \vec{X}_\delta(t) - \vec{X}(t) \right| \quad (8)$$

$$\vec{X}_1 = \vec{X}_\alpha(t) - \vec{A}_1 \cdot \vec{D}_\alpha, \quad \vec{X}_2 = \vec{X}_\beta(t) - \vec{A}_2 \cdot \vec{D}_\beta,$$
$$\vec{X}_3 = \vec{X}_\delta(t) - \vec{A}_3 \cdot \vec{D}_\delta \quad (9)$$

$$\vec{X}(t+1) = \frac{\vec{X}_1 + \vec{X}_2 + \vec{X}_3}{3} \quad (10)$$

B. IMPROVE GWO ALGORITHM (IGWO)

For the GWO algorithm, the convergence factor a linearly decreases from 2 to 0 with the number of iterations. The convergence process of the algorithm is not linearly convergent. A nonlinear convergence factor based on the tangent trigonometric function is adopted in this paper as follow:

$$a = a_{\text{initial}} - (a_{\text{initial}} - a_{\text{final}}) \times \tan(\frac{1}{\varepsilon} \cdot \frac{l}{l_{\max}}\pi) \quad (11)$$

where $a_{initial}$, a_{final} are initial value and final value and final value of the convergence factor a respectively, ε is the adjustment coefficient, this paper takes $\varepsilon = 4$, l is the current iteration number, $l_{\max}$ is the maximum number of iterations.

At the same time, the algorithm needs to track the maximize power point (MPP) in real time. Since the output power of the PV arrays also changes when the external environment such as irradiance and temperature changes, in order to avoid the algorithm falling into an infinite cycle, it is necessary to restart the algorithm for power tracking. When the output power variation satisfies (12), the algorithm re-initialized.

$$\frac{|P_{\text{real}} - P_m|}{P_m} > \Delta P \quad (12)$$

where P_{real} is the actual output power of the PV arrays, P_m is the output power of the PV arrays at the MPP under the current working condition, and ΔP is the threshold for the output power change of the PV arrays, this paper set to 0.2.

The flow chart of the proposed MPPT algorithm is shown in Fig.4.

It is worth noting that the "duty cycle x_i" mentioned here is not a true duty cycle, but a carrier x_i with a linear function relationship with the true duty cycle. In this paper, the triangular wave is used as the modulation wave. The transformation
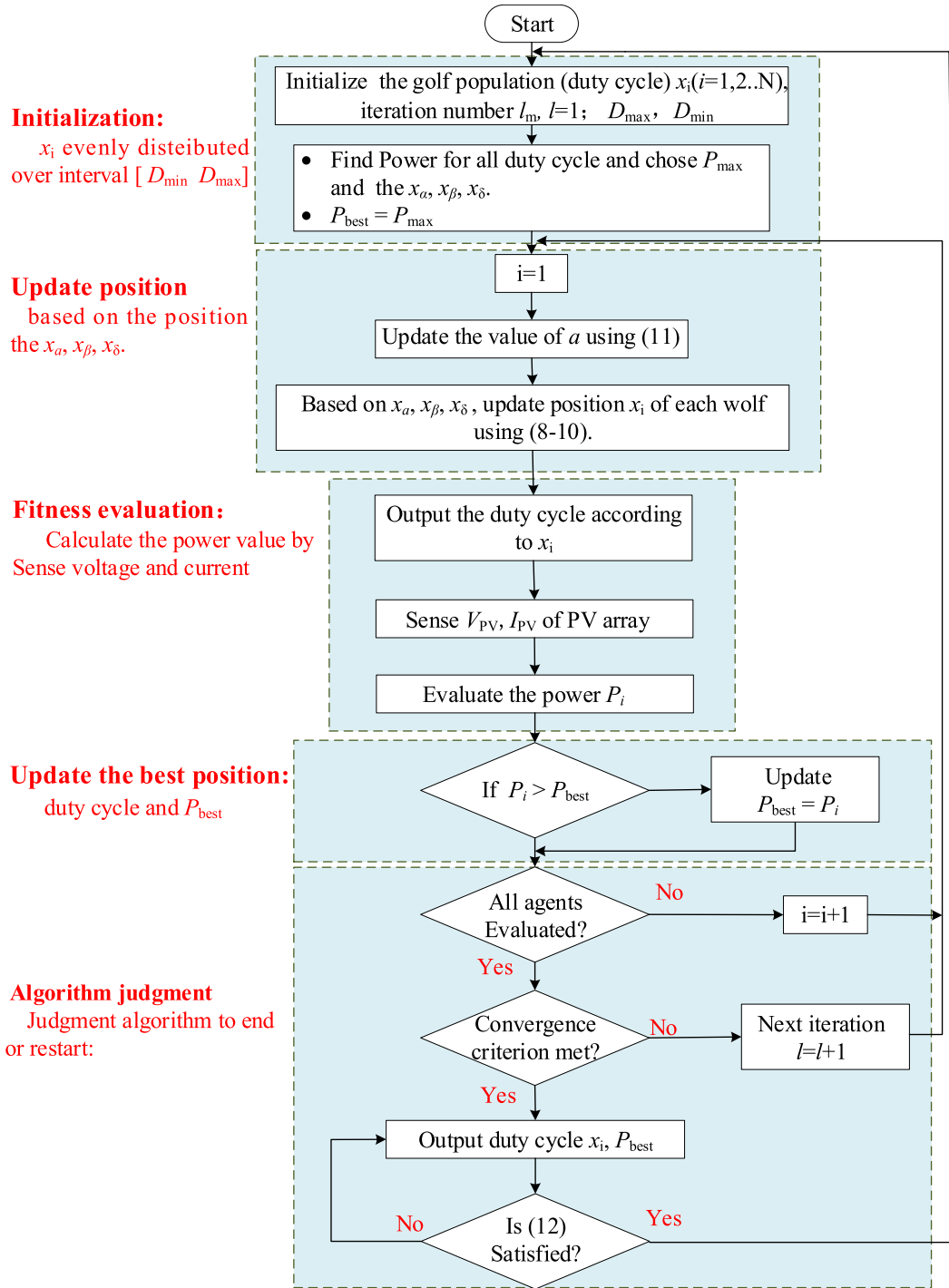
Initialization:
 x_i evenly disteibuted over interval [D_{min} D_{max}]

Update position
 based on the position the x_α, x_β, x_δ.

Fitness evaluation:
 Calculate the power value by Sense voltage and current

Update the best position:
 duty cycle and P_{best}

Algorithm judgment
 Judgment algorithm to end or restart:

FIGURE 4. The flow chart of the proposed MPPT algorithm.

relationship of the carrier x_i and the duty cycle d is shown in Fig.5.

Hence, the mathematical relationship between the carrier x_i and the duty cycle d can be obtained:

$$d = \frac{A_C + x_i}{2A_C} = \frac{1}{2} + \frac{x_i}{2A_C} \qquad (13)$$

where A_C is set to 1.

IV. THE CONVERGENCE ANALYSIS OF IGWO ALGORITHM
The convergence is one of the important characteristics of algorithm. Whether the algorithm converges can be analyzed and proved with the help of mathematics theoretical knowledge. Markov process and convergence in probability have been widely applied [34], [35]. The update process of the IGWO algorithm only considers the position of α, β, δ and prey after the last iteration, and has nothing to
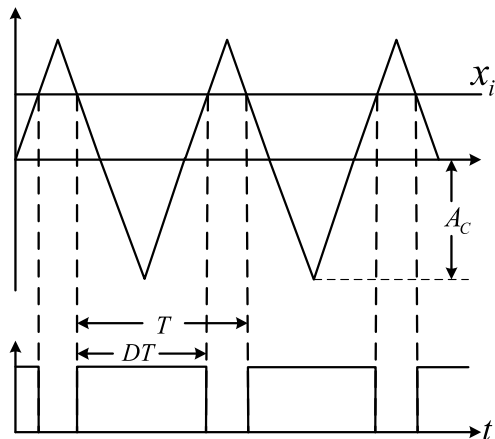
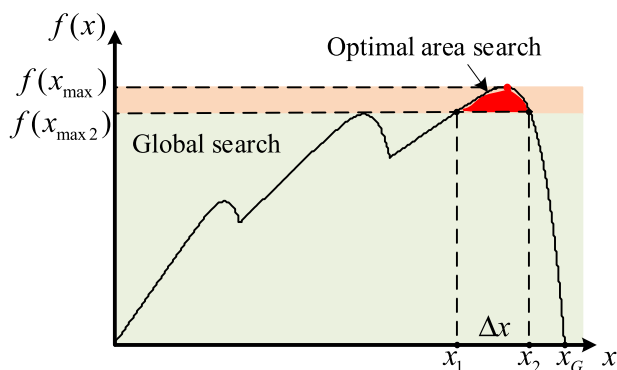**FIGURE 5.** The transformation relationship diagram.

FIGURE 6. The optimization process of algorithm.

do with the original state. This feature exactly constitutes a Markov process. Therefore, the optimization process of IGWO algorithm is transformed into Markov process, and the convergence of the IGWO algorithm is analyzed with convergence in probability. The optimization process is divided into two stages, namely, the global search and the optimal area search. As shown in Fig.6, The $f(x_{max})$ and $f(x_{max2})$ represent the optimal value and the suboptimal value of the objective function, respectively. In two-dimensional (2-D) graphs, the independent variable and the dependent variable have a one-to-one correspondence. Therefore, the formula of the algorithm in the following analysis uses algebraic form rather than vector form.

A. GLOBAL SEARCH ANALYSIS

At the beginning of the global search, the initial position of the wolves needs to be randomly initialized, and the probability that it is located in the interval $[x_1, x_2]$ denoted by:

$$P_G = \frac{\Delta x}{x_G} \quad (14)$$

For any iteration, the update range of the wolf pack position denoted by:

$$-\frac{7}{3}(x_\alpha + x_\beta + x_\delta) \le x \le \frac{1}{3}(x_\alpha + x_\beta + x_\delta) + 12x(t) \quad (15)$$

where $x_\alpha, x_\beta, x_\delta$ are the positions of a, β, and δ, respectively; the range length is recorded as x_u, and $x(t)$ represents the position of the gray wolf before iteration.

There are three types of relationships between the update range and the optimal region in any one iteration, namely, separation, partial inclusion, and complete inclusion (this relationship is classified as optimal search).

1) PARTIAL INCLUSION

In this case, the probability of being able to move to the optimal region in one step denoted by:

$$P_{x \to \Delta x} = P_G \cdot \sum_{i=1}^{N} \frac{x_c}{N x_u} \quad (16)$$

where N is the number of gray wolves; and x_c is the length of the overlapping part of x_u and Δx. After k iterations, the probability that the gray wolves cannot reach the optimal region is:

$$\lim_{k \to \infty} \prod_{i=m}^{k} (1 - P_{x \to \Delta x}) = \lim_{k \to \infty} (1 - P_G \cdot \sum_{i=1}^{N-1} \frac{x_c}{N x_u})^k = 0 \quad (17)$$

2) SEPARATION

The probability of separation after iteration denoted by:

$$P_{x_G \to \Delta x} = \frac{x_G - \Delta x}{x_G} \quad (18)$$

After k iterations, the probability of the separation relationship is:

$$\lim_{k \to \infty} P_{x_G - \Delta x} = \lim_{k \to \infty} \frac{x_G - \Delta x}{x_G} = 0 \quad (19)$$

3) COMPLETE INCLUSION

When this happens, it means that the update range is completely within the optimal area. No matter what happens, after k iteration, the update range is still in the optimal area. Therefore, this type belongs to the optimal area search category.

In summary, the grey wolves must converge to the optimal region through iterations.

B. OPTIMAL AREA SEARCH ANALYSIS

The probability that grey wolves will find the optimal value (prey) in one step in this area denoted by:

$$P_{x \to x_{max}} = P_o \cdot \sum_{i=1}^{N} \frac{x_{c1}}{N \Delta x_{max}} \quad (20)$$

where x_{c1} is the length of the overlapping part of x_u and Δx_{max}; The range of Δx_{max} is $[x_{max}-\mu, x_{max} + \mu]$, μ is the error limit; When x is in this range, it can be considered that a global optimum has been found. P_o can be expressed as:

$$P_O = \frac{\Delta x_{max}}{\Delta x} \quad (21)$$

Similar to global search analysis, the grey wolves must converge to Δx_{max} in the optimal region.
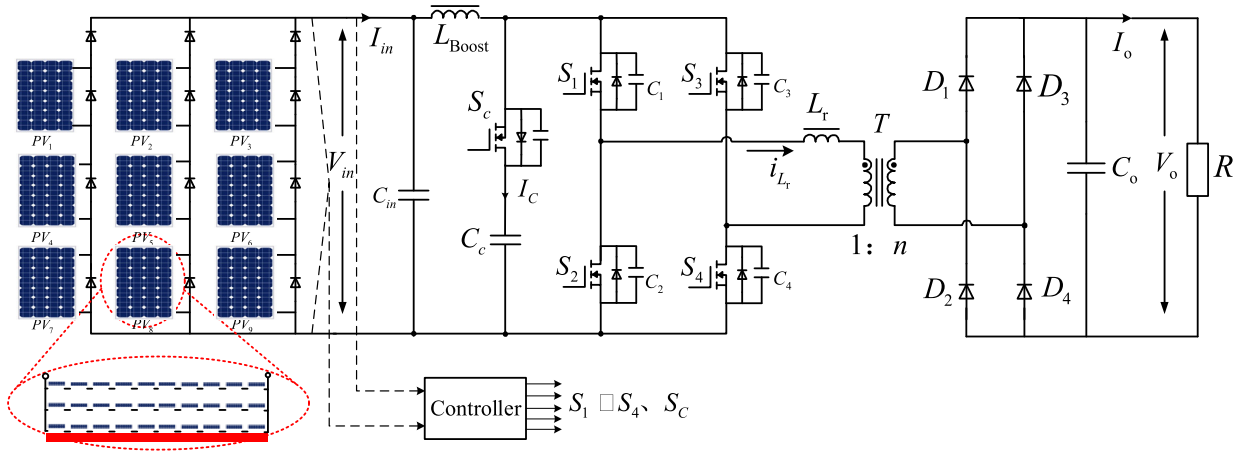
FIGURE 7. PV system with a BFBIC converter with the proposed control scheme.

TABLE 1. Main parameter of the MSX-60W.

Parameter	Symbol	Value
Maximum power	P_{MPP}	59.85W
Maximum power voltage	V_{MPP}	17.1V
Maximum power current	I_{MPP}	3.5A
Open-circuit voltage	V_{OC}	21.1V
Shout-circuit current	I_{SC}	3.8A
Temperature coefficient of V_{OC}	K_V	-80mV/^{0}C
Temperature coefficient of I_{SC}	K_I	0.065%/^{0}C

FIGURE 8. The linear and nonlinear convergence factor curves.
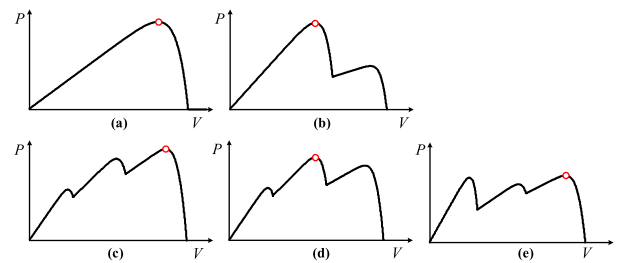
FIGURE 9. Different PSC patterns for adopted PV arrays.

V. SIMULATION RESULTS AND ANALYSIS

To verify the performance of the proposed control strategy, a PV system consisting of series-parallel PV arrays with the BFBIC converter was established as depicted in Fig.7. The PV array adopts the structure of 3×3, in which the first and second column sub-arrays contain 10×3 sub-modules, and the third column sub-arrays is 10×4 sub-modules. The model number of each submodule is MSX-60W, and some parameters are shown in Table 1. Main parameters of the BFBIC converter are $C_{in} = 100\mu F$, $C_0 = 200\mu F$, and $L = 6mH$. The switching frequency is 10 kHz.

The linear and nonlinear convergence factor curves are shown in Fig.8. In the initial stage of the iteration, the improved convergence factor has a small absolute value, which is conductive to finding the global optimal solution. In the later stage of iteration, the absolute value of the slope is large, which improves the speed and capability of exploitation. Hence, the IGWO has the better of capability exploration and exploitation.

To evaluate the performance of the IGWO algorithm, it has been compared with conventional P&O, PSO, ABC, WSSA, SSA-PSO, SSA-GWO, EGWO. In addition to P&O, other algorithms adapt a uniform number of iterations and the number of particles. The parameter settings of each algorithm are shown in Table 2. It is worth noting that some algorithms
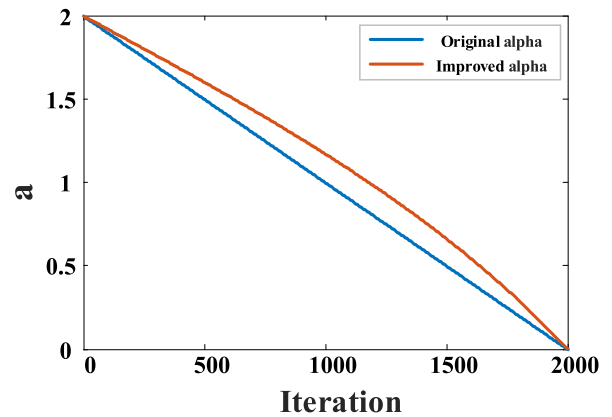
are explained: the SSA-GWO algorithm adopts GWO to update the leader of SSA algorithm, the SSA-PSO algorithm is combined by SSA and PSO algorithm, and randomly selects an algorithm for power tracking during each iteration, the EGWO algorithm only uses gray wolf α and gray wolf β to update algorithm. For the WSSA, the linearly decreasing inertia weight is adopted to update the followers of the SSA, namely:

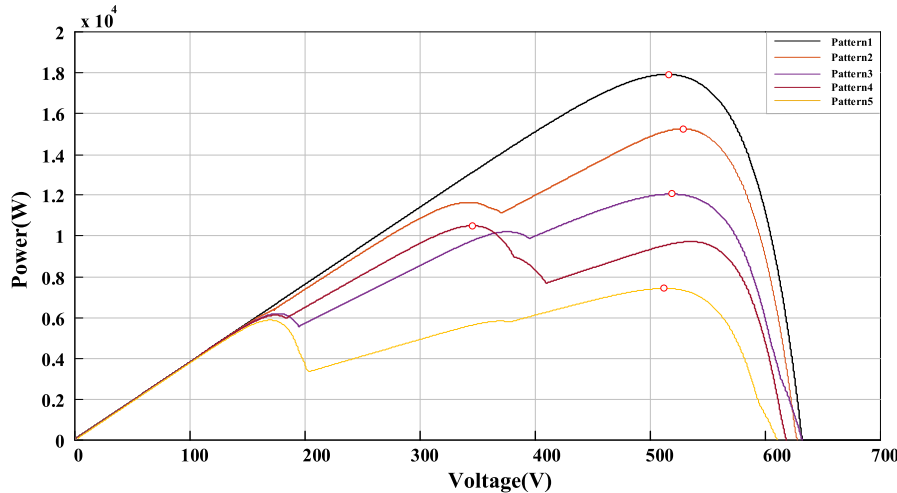$$w = 0.9 - \frac{(0.9 - 0.2) \times (l - 1)}{iter_{max}} \qquad (22)$$

FIGURE 10. The P-V characteristic curves.

TABLE 2. Parameter settings for different algorithms.

Algorithm	Parameter setting
P&O	$\Delta D = 0.01$
PSO	Inertia weight w Self-adaption, $C_1 = C_2 = 2$
ABC	Limit=3
WSSA	Inertia weight w and C_1: Self-adaption
SSA-GWO	a and C_1: Self-adaption
SSA-PSO	Inertia weight w and C_{1SSA}: Self-adaption, $C_{1PSO} = C_{2\,PSO} = 2$
EGWO	a: Self-adaption
IGWO	a: Self-adaption

where l is the current number of iterations and $iter_{max}$ is the maximum number of iterations.

Since the PV arrays are equipped with the bypass diode and the blocking diode, for the PV arrays of 3×3, the P-V curve of the PV arrays has at most three peaks, regardless of the change in the irradiance of each sub-arrays, which are roughly divided into nine types. Hence, the five different P-V curves were designed taking into account the actual environment in which the PV array is located and its abrupt changes. The irradiation patterns of the PV arrays are given in Table 3, in which Pattern 1 - Pattern 5 corresponds to Fig.9 (a)-(e). The corresponding P-V characteristic curves are shown in Fig.10, the red circle indicates the MPP of each P-V curve.

A. STATIC PERFORMANCE OF IGWO UNDER PSCS
As can be seen from Fig.10, the P-V curve of Pattern 4 has two similar extreme points, which are 10550W and 9825W, respectively. When verifying the performance of the control strategy in a static environment, the simulation based on the irradiance shown in Pattern 7 can better verity the adaptability and accuracy of each algorithm.

The simulation results of different algorithm are shown in Fig.11, and Table 4 shows the statistical results. Including the

tracking efficiency (η) and tracking time (T). Compared to the other algorithm, although the P&O algorithm can run stably at 0.3s, its GMPPT efficiency is only 73.93%. Several intelligent algorithms have better performance and their tracking efficiency is above 99.50%. Meanwhile, the proposed IGWO algorithm shortens the tracking time by about 30%, which indicates IGWO has faster tracking speed compared to the other algorithms.

B. DYNAMIC PERFORMANCE OF IGWO UNDER PSCS
In order to further verify the dynamic stability of the IGWO based GMPPT method and the clearer observation of the curve change, this paper adopts the change sequence of Pattern 1 – Pattern 4 – Pattern 2 – Pattern 5 – Pattern 3 – Pattern 1 to verity the simulation. To ensure that the MPPT algorithm were able to track the new MPP under changing irradiance, a re-initialization strategy was implemented. The time interval of the change of the irradiance is 0.5s. The simulation results of each algorithm are shown in Fig.12, which mainly includes the output power waveform and the "duty cycle" waveform. The statistical results are given in Table 5.

Cases 1 and Cases6: Pattern 1 was employed, the interval corresponds to $0 < t < 0.5s$ and $2.5s < t < 3s$, respectively.

Between these intervals, the irradiation of PV arrays is 1000W/m^2, the MPP is about 17955W. It can be seen from Fig.12(a) that the P&O algorithm can track MPP at 0.2s, and its efficiency was about 99.14%, but the output power has a large oscillation around the maximum power. Although the PSO and ABC algorithms have improved tracking accuracy and efficiency to some extent, they have sacrificed tracking time. The improved SSA further improves the tracking time, tracking accuracy and efficiency. The efficiency of WSSA, SSA-GWO, SSA-PSO and EGWO was 99.71%, 99.98%,, 99.89% and 99.82%, respectively. In contrast, the proposed IGWO was better than the other six algorithms. The IGWO

TABLE 3. Irradiance patterns of PV arrays.

Pattern	P_{mpp} (w)	Irradiance of PV arrays (W/m^2)								
		PV_1	PV_2	PV_3	PV_4	PV_5	PV_6	PV_7	PV_8	PV_9
1	17955	1000	1000	1000	1000	1000	1000	1000	1000	1000
2	15361	1000	1000	1000	1000	900	1000	800	800	800
3	12158	1000	1000	1000	600	600	1000	300	600	1000
4	10550	1000	1000	1000	800	1000	800	600	300	600
5	7586	1000	1000	1000	400	300	600	300	300	600
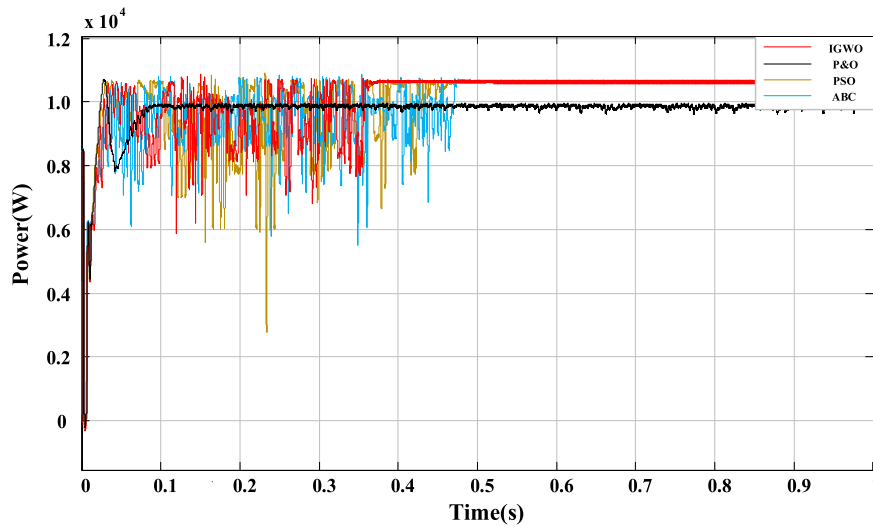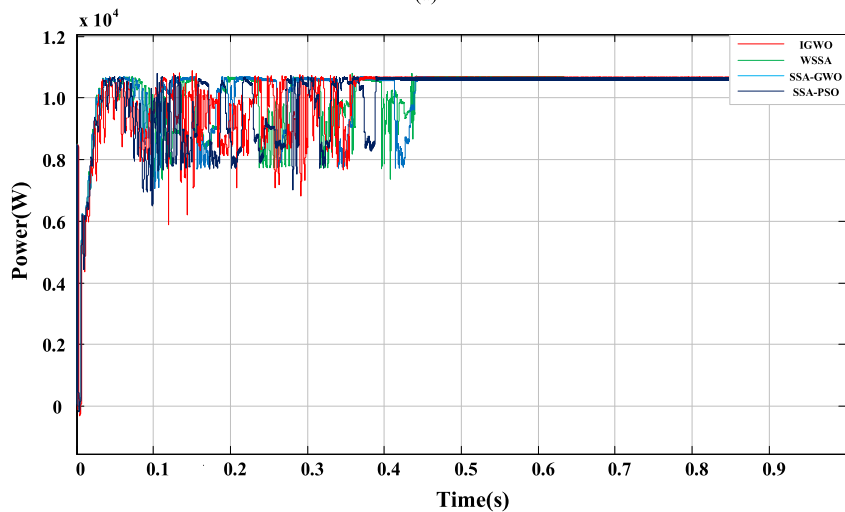
FIGURE 11. Output waveforms of the PV system using different MPPT algorithms: (a) Output waveforms of the basic MPPT algorithm, (b) Output waveforms of the improve MPPT algorithm.

was slightly lower in tracking efficiency than the SSA-GWO algorithm, but it improved the tracking time by 25%.

Cases 2: at t = 0.5s, the irradiation changed suddenly and Pattern 4 was employed, the interval corresponds to 0.5s < t < 1s.

At t = 0.5s, the PV arrays operated under the PSC. At this time, the algorithms successfully detected partial shade and entered the re-initialization stage. As depicted in

Fig.12, the P&O algorithm was trapped in a local optimum when operated in Pattern 4. Compared with the traditional algorithms, the tracking efficiency of the six bionic intelligent algorithms were all above 99.5%. Among them, the tracking efficiency and tracking speed of the IGWO algorithm had superiority.

It is worth noting that, compared to the waveform in section 5.1, the tracking time of each algorithm has been
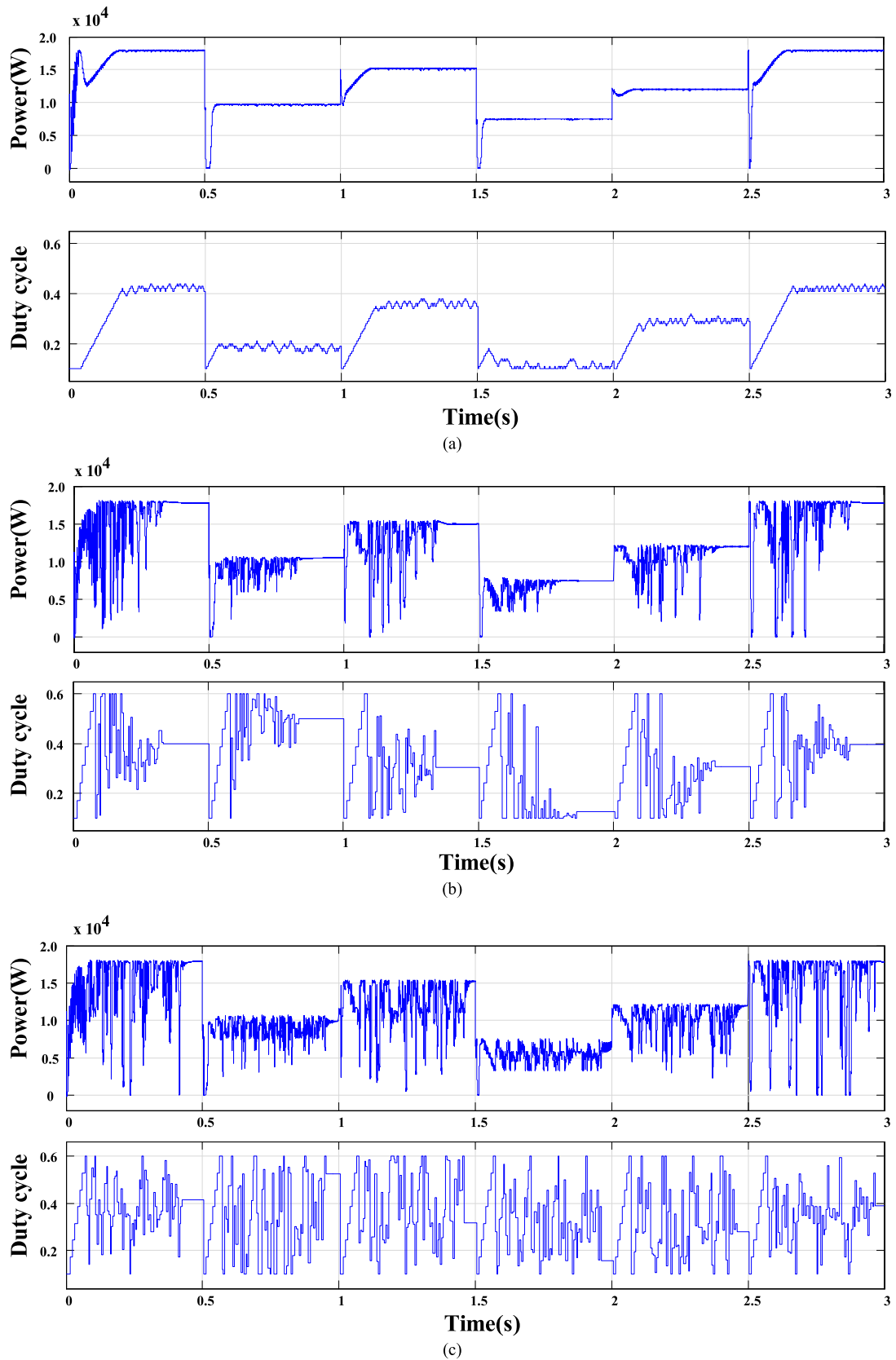
FIGURE 12. Dynamic Performance under PSCs: (a) perturb and observe(P&O), (b) particle swarm optimization (PSO), (c) artificial bee colony (ABC), (d) adapt Inertia weight salp swarm algorithm (WSSA), (e) SSA with grey wolf optimizer (SSA-GWO), (f) SSA with PSO (SSA-PSO), (g) the proposed method (IGWO), (h) enhanced GWO (EGWO).

FIGURE 12. *(Continued.)* Dynamic Performance under PSCs: (a) perturb and observe(P&O), (b) particle swarm optimization (PSO), (c) artificial bee colony (ABC), (d) adapt Inertia weight salp swarm algorithm (WSSA), (e) SSA with grey wolf optimizer (SSA-GWO), (f) SSA with PSO (SSA-PSO), (g) the proposed method (IGWO), (h) enhanced GWO (EGWO).

(g)

(h)

FIGURE 12. *(Continued.)* Dynamic Performance under PSCs: (a) perturb and observe(P&O), (b) particle swarm optimization (PSO), (c) artificial bee colony (ABC), (d) adapt Inertia weight salp swarm algorithm (WSSA), (e) SSA with grey wolf optimizer (SSA-GWO), (f) SSA with PSO (SSA-PSO), (g) the proposed method (IGWO), (h) enhanced GWO (EGWO).
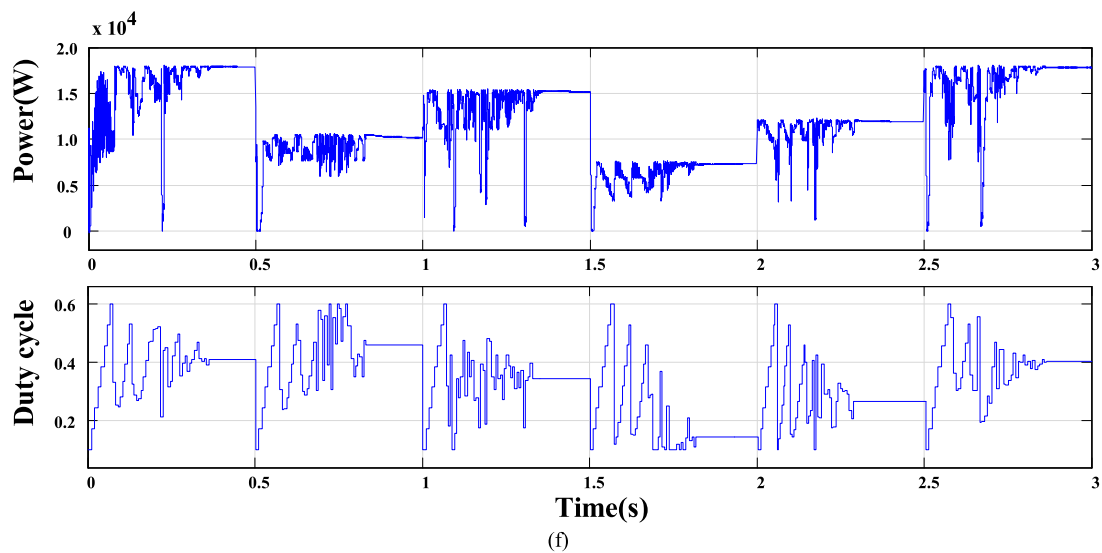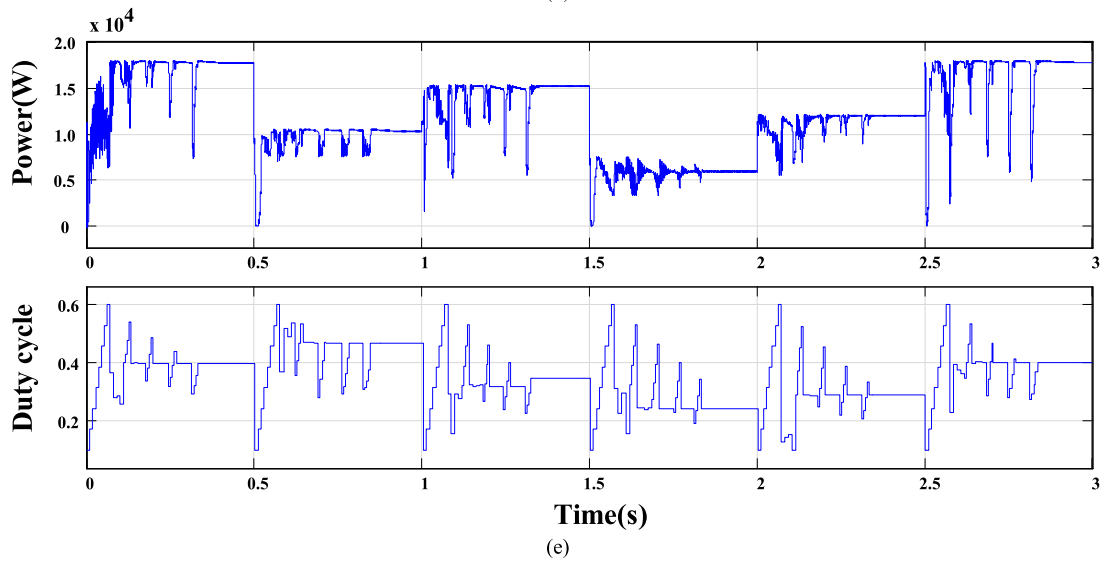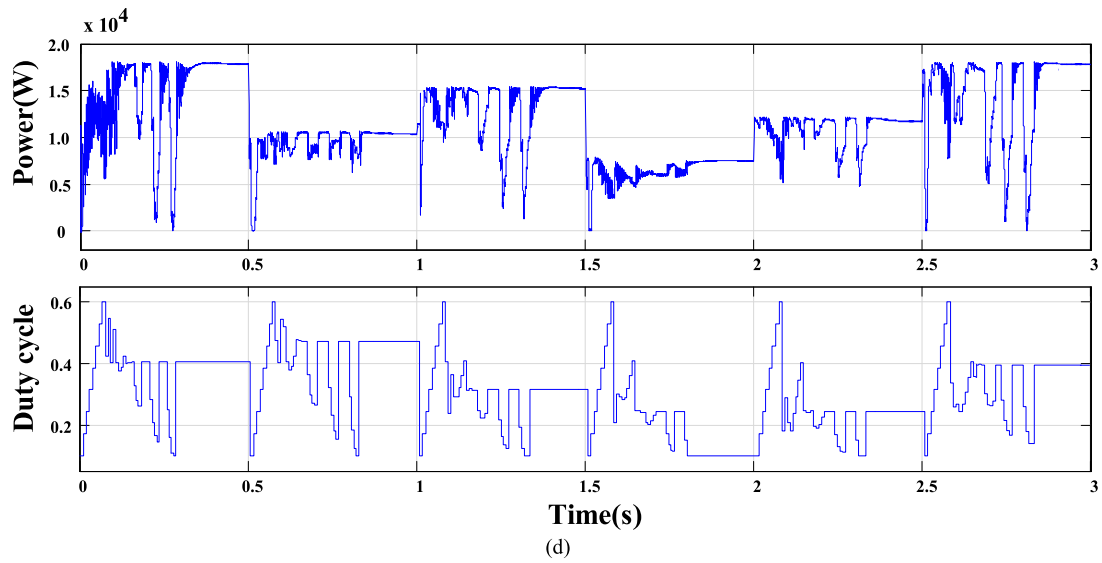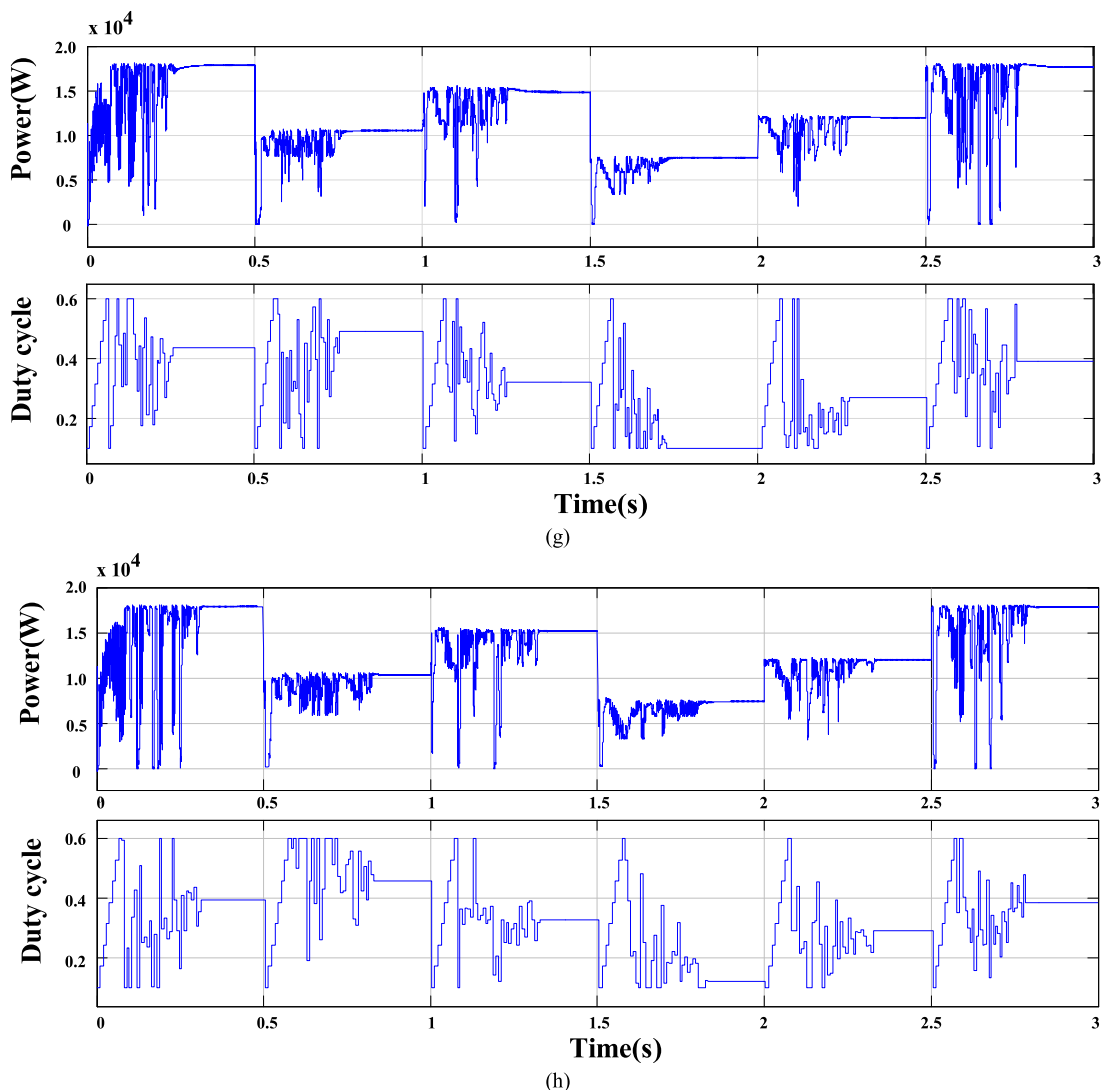
TABLE 4. The statistical results of the different MPPT algorithms.

Algorithm	P_{max}(W)	η	T (s)
P&O	9700	91.94%	0.19
PSO	10520	99.71%	0.46
ABC	10502	99.54%	0.47
WSSA	10523	99.74%	0.44
SSA-GWO	10533	99.84%	0.43
SSA-PSO	10520	99.71%	0.39
IGWO	10530	99.81%	0.35

reduced, indicating that the initial state of the topology has a certain effect on the algorithm.

Cases 3: at t = 1s, the irradiation changed suddenly and Pattern 2 was employed, the interval corresponds to 1s < t < 1.5s.

At this stage, the operating conditions of the PV array were changed, namely, the mutation from Pattern 4 to Pattern 2. It can be seen from Table 5 that each algorithm can effectively track the MPP. Although the PV system are in PSC, the P&O algorithm still track MPP, with an efficiency of 98.04%. The reason for this phenomenon is that the tracking process of P&O algorithm starts form the right end of the P-V curve, namely the open circuit voltage. If the right-most maximum point of the P-V curve exactly corresponds to MPP, the traditional P&O algorithm can track effectively, but its oscillation is large, and the tracking time was related to the perturbation quantity.

Cases 4: at t = 1.5s, the irradiation changed suddenly and Pattern 5 was employed, the interval corresponds to 1.5s < t < 2s.

In Pattern 5, MPP was located at the rightmost pole of the P-V curve, and its corresponding maximum power

TABLE 5. The statistical results of different MPPT algorithms.

| Cases	Index	P&O	PSO	ABC	WSSA	SSA-GWO	SSA-PSO	EGWO	IGWO
Cases 1 P_{real}=17955W	P_m(W)	1.7802e+04	1.7901e+04	1.7908e+04	1.7903e+04	1.7945e+04	1.7936e+04	1.7924e+04	1.7947e+04
	η	99.14%	99.69%	99.73%	99.71%	99.94%	99.89%	99.82%	99.95%
	T (s)	0.2	0.34	0.43	0.29	0.34	0.37	0.32	0.27
Cases 2 P_{real}=10550W	P_m(W)	9.7455e+03	1.0505e+04	1.0518e+04	1.0525e+04	1.0503e+04	1.0529e+04	1.0486e+04	1.0532e+04
	η	92.37%	99.57%	99.69%	99.76%	99.55%	99.80%	99.39%	99.82%
	T (s)	0.05	0.34	0.46	0.33	0.35	0.34	0.33	0.27
Cases 3 P_{real}=15361W	P_m(W)	1.5060e+04	1.5245e+04	1.5168e+04	1.5286e+04	1.5316e+04	1.5236e+04	1.5287e+04	1.5297e+04
	η	98.04%	99.24%	98.74%	99.51%	99.70%	99.18%	99.51%	99.58%
	T (s)	0.13	0.35	0.47	0.34	0.34	0.34	0.31	0.27
Cases 4 P_{real}=7586W	P_m(W)	7.2939e+03	7.4401e+03	7.3397e+03	7.4477e+03	---	7.4370e+03	7.4127e+03	7.4753e+03
	η	96.15%	98.07%	96.75%	98.17%	---	98.03%	97.71%	98.54%
	T (s)	0.14	0.37	0.47	0.31	---	0.32	0.32	0.24
Cases 5 P_{real}=12158W	P_m(W)	1.1907e+04	1.2087e+04	1.2011e+04	1.2095e+04	1.2118e+04	1.2070e+04	1.2081e+04	1.2128e+04
	η	97.93%	99.4%	98.79%	99.48%	99.67%	99.27%	99.36%	99.75%
	T (s)	0.12	0.38	0.46	0.34	0.34	0.30	0.32	0.28
Cases 6 P_{real}=17955W	P_m(W)	1.7802e+04	1.7932e+04	1.7900e+04	1.7928e+04	1.7952e+04	1.7928e+04	1.7938e+04	1.7946e+04
	η	99.14%	99.87%	99.69%	99.84%	99.98%	99.84%	99.90%	99.94%
	T (s)	0.16	0.38	0.47	0.33	0.34	0.37	0.30	0.28
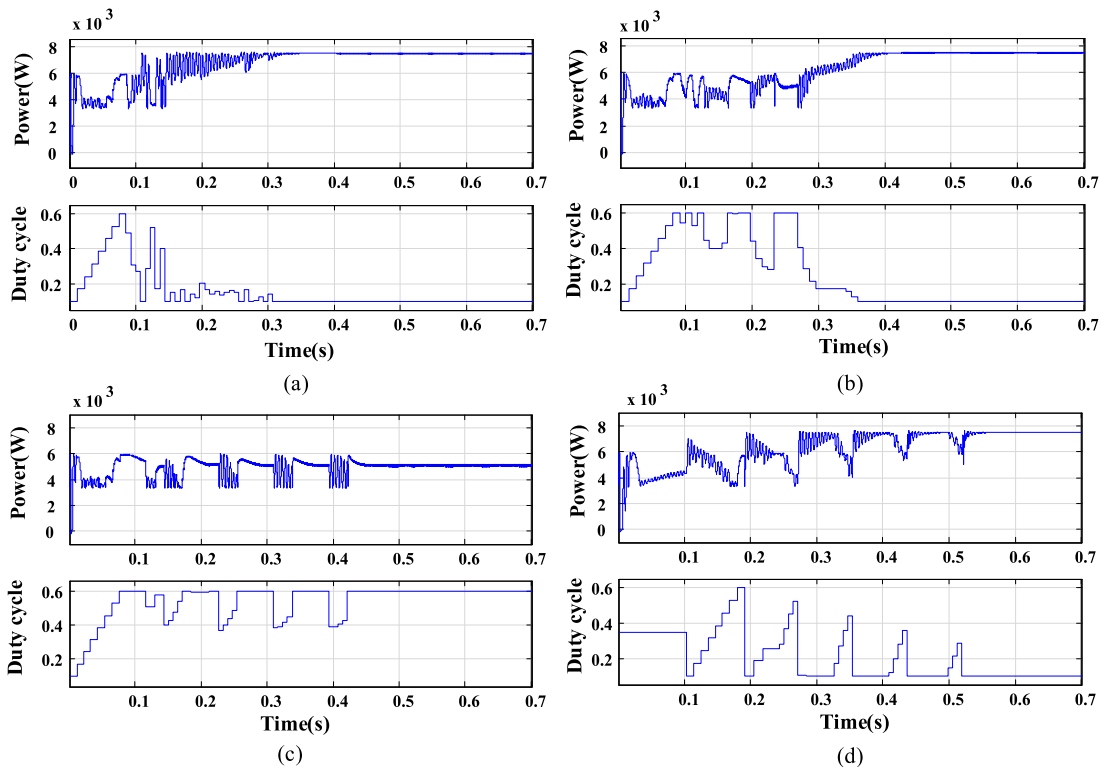
FIGURE 13. Output waveforms of the PV system using different MPPT algorithms under Pattern5: (a) the proposed algorithm (IGWO), (b) adapt Inertia weight salp swarm algorithm (WSSA), (c) SSA with grey wolf optimizer (SSA-GWO), (d) Delayed 0.1s initializing SSA-GWO.

was 7500W, and the theoretical value of ''duty cycle'' was 0.1. According to the above analysis, the traditional P&O algorithm can still track the MPP and fluctuate on both sides of the MPP, and its efficiency was 96.15%. Except for the SSA-GWO algorithm (detailed analysis later), all

other bionic intelligent algorithms can effectively track MPP. Among them, IGWO algorithm has better performance.

Cases 5: at t = 2s, the irradiation changed suddenly and Pattern 3 was employed, the interval corresponds to 2s < t < 2.5s.

It can be seen from Fig. 12 and Table 5 that each algorithm can track MPP in this interval. In terms of tracking efficiency, the ABC algorithm was the best, but its tracking time was the longest and the power fluctuations was large during the tracking process. The tracking efficiency of the IGWO was only 0.04% smaller than that of the ABC algorithm, but the tracking time was shortened by nearly half.

In order to analyze the problems of SSA-GWO algorithm in the Pattern 5, the IGWO, SSA-GWO, WSSA were used for static simulation under this working condition, as show in Fig.13. The same parameters were used in the comparative simulation, including initialization, number of iterations, and number of particles. It can be seen from Fig.13(a), (b) that IGWO and WSSA show strong global exploration ability after initialization. After a short search time, the particles almost completely converged near MPP. However, for the SSA-GWO algorithm, as shown in Fig.13 (c), although the GWO was used to optimize the leader, it does not have the strong global exploration ability like the WSSA. To further analyze the influence of the topology working state before initialization on the SSA-GWO, Set the fixed ''duty cycle'' to run for 0.1s and then initialize algorithm. The waveform is shown in Fig.13 (d). Obviously, when the optimal value was at the boundary of the particle search range, the working state of the topology has a significant influence on the performance of the SSA-GWO, which has no limitation on IGWO. Although the algorithm has limitations in searching for boundary optimal values, it cannot be denied that it still has good performance when searching for non-boundary optimal values. For example, in Pattern 1 and Pattern 3, the SSA-GWO is slightly better in tracking efficiency than IGWO, but the required tracking time is much longer than IGWO.

VI. CONCLUSIONS

In this paper, based on the BFBIC topology and considering the sudden changes in the external environment, a GMPPT control strategy based on the proposed IGWO algorithm is put forward. In the strategy, a nonlinear tangent trigonometric function as a convergence factor is integrated into the GWO algorithm. In addition, the active-clamp circuit and phase-shift are used to implement the soft switch technology. The convergence of IGWO is analyzed by using Markov process and convergence in probability. Furthermore, the MPPT results tested on the PV system simulation platform validated the effectiveness and superiority of the proposed IGWO MPPT algorithm. The causes of tracking failure of SSA-GWO algorithm in Pattern 5 are further compared and analyzed. It is concluded that IGWO has the following advantages:

1) The MPP can be tracked stably and effectively under different PSCs;

2) Compared with other algorithms, the proposed control method based on IGWO is equipped with faster tracking speed and high reliability;

3) The proposed IGWO MPPT method can effectively realize ZVS of active clamp switch and bridge switch.

REFERENCES

[1] Y. Liu, H. Abu-Rub, and B. Ge, "Front-end isolated quasi-Z-source DC–DC converter modules in series for high-power photovoltaic systems—Part I: Configuration, operation, and evaluation," *IEEE Trans. Ind. Electron.*, vol. 64, no. 1, pp. 347–358, Jan. 2017.

[2] Y. Liu, H. Abu-Rub, and B. Ge, "Front-end isolated quasi-Z-source DC–DC converter modules in series for high-power photovoltaic systems—Part II: Control, dynamic model, and downscaled verification," *IEEE Trans. Ind. Electron.*, vol. 64, no. 1, pp. 359–368, Jan. 2017.

[3] Y. Yu, G. Konstantinou, B. Hredzak, and V. G. Agelidis, "Power balance of cascaded H-Bridge multilevel converters for large-scale photovoltaic integration," *IEEE Trans. Power Electron.*, vol. 31, no. 1, pp. 292–303, Jan. 2016.

[4] A. Blinov, R. Kosenko, A. Chub, and D. Vinnikov, "Snubberless boost full-bridge converters: Analysis of soft switching performance and limitations," *Int. J. Circuit Theory Appl.*, vol. 47, no. 6, pp. 884–908, Jun. 2019.

[5] M.-K. Nguyen, T.-D. Duong, Y.-C. Lim, and Y.-J. Kim, "Isolated boost DC–DC converter with three switches," *IEEE Trans. Power Electron.*, vol. 33, no. 2, pp. 1389–1398, Feb. 2018.

[6] X. Hu and C. Gong, "A high gain input-parallel output-series DC/DC converter with dual coupled inductors," *IEEE Trans. Power Electron.*, vol. 30, no. 3, pp. 1306–1317, Mar. 2015.

[7] L. Zhu, "A novel soft-commutating isolated boost full-bridge ZVS-PWM DC–DC converter for bidirectional high power applications," *IEEE Trans. Power Electron.*, vol. 21, no. 2, pp. 422–429, Mar. 2006.

[8] R.-Y. Chen, T.-J. Liang, J.-F. Chen, R.-L. Lin, and K.-C. Tseng, "Study and implementation of a current-fed full-bridge boost DC–DC converter with zero-current switching for high-voltage applications," *IEEE Trans. Ind. Appl.*, vol. 44, no. 4, pp. 1218–1226, Jul./Aug. 2008.

[9] J.-H. Lee, J.-J. Jung, and S.-K. Sul, "Balancing of submodule capacitor voltage of hybrid modular multilevel converter under DC-bus voltage variation of HVDC system," *IEEE Trans. Power Electron.*, vol. 34, no. 11, pp. 10458–10470, Nov. 2019.

[10] Y. Liang, J. Liu, T. Zhang, and Q. Yang, "Arm current control strategy for MMC-HVDC under unbalanced conditions," *IEEE Trans. Power Del.*, vol. 32, no. 1, pp. 125–134, Feb. 2017.

[11] M. Saeedifard and R. Iravani, "Dynamic performance of a modular multilevel Back-to-Back HVDC system," *IEEE Trans. Power Del.*, vol. 25, no. 4, pp. 2903–2912, Oct. 2010.

[12] O. A. Ahmed and J. A. M. Bleijs, "High-efficiency DC-DC converter for fuel cell applications: Performance and dynamic modeling," in *Proc. IEEE Energy Convers. Congr. Exposit. ECCE*, Sep. 2009, pp. 67–74.

[13] A. Amir, A. Amir, H. S. Che, A. Elkhateb, and N. A. Rahim, "Comparative analysis of high voltage gain DC-DC converter topologies for photovoltaic systems," *Renew. Energy*, vol. 136, pp. 1147–1163, Jun. 2019.

[14] M. E. Başoğlu and B. Çakır, "Comparisons of MPPT performances of isolated and non-isolated DC–DC converters by using a new approach," *Renew. Sustain. Energy Rev.*, vol. 60, pp. 1100–1113, Jul. 2016.

[15] R. Reshma Gopi and S. Sreejith, "Converter topologies in photovoltaic applications—A review," *Renew. Sus. Energ. Rev.*, vol. 94, pp. 1–14, Oct. 2018.

[16] R. Watson and F. C. Lee, "A soft-switched, full-bridge boost converter employing an active-clamp circuit," in *Proc. Rec. 27th Annu. IEEE Power Electron. Spec. Conf. (PESC)*, vol. 2, Jan. 1996, pp. 1948–1954.

[17] S. Ikeda and F. Kurokawa, "Isolated and wide input ranged boost full bridge DC-DC converter with low loss active snubber," in *Proc. IEEE Energy Convers. Congr. Exposit. (ECCE)*, Oct. 2017, pp. 2213–2218.

[18] R. Anand, T. S. A. Samuel, and P. M. Mary, "Improved dynamic response of isolated full bridge DC to DC converter using BATA optimization tuned fuzzy sliding mode controller for solar applications," *Int. J. Hydrogen Energy*, vol. 42, no. 34, pp. 21648–21658, Aug. 2017.

[19] Z. Zhang, H. R. Nielsen, M. A. E. Andersen, and O. C. Thomsen, "Dual-input isolated full-bridge boost DC–DC converter based on the distributed transformers," *IET Power Electron.*, vol. 5, no. 7, pp. 1074–1083, Aug. 2012.

[20] P. Xuewei, A. Kumar Rathore, and U. R. Prasanna, "Novel soft-switching snubberless naturally clamped current-fed full-bridge front-end-converter-based bidirectional inverter for renewables, microgrid, and UPS applications," *IEEE Trans. Ind. Appl.*, vol. 50, no. 6, pp. 4132–4141, Dec. 2014.

[21] L. R. de Oliveira, P. S. N. Filho, T. A. dos Santos Barros, M. G. Villalva, and E. Ruppert, "Input voltage regulation of an isolated full-bridge boost converter fed by a photovoltaic device with the state-space feedback control method," in *Proc. Brazilian Power Electron. Conf.*, Oct. 2013, pp. 595–600.

[22] R. Zhang, H. Xu, and Y. Wang, "A dynamic priority factor loop for fast voltage equalization applied to high power density DC–DC converter system," *IEEE Trans. Power Electron.*, vol. 35, no. 1, pp. 198–207, Jan. 2020.

[23] H. Li, D. Yang, W. Su, J. Lu, and X. Yu, "An overall distribution particle swarm optimization MPPT algorithm for photovoltaic system under partial shading," *IEEE Trans. Ind. Electron.*, vol. 66, no. 1, pp. 265–275, Jan. 2019.

[24] S. Mirjalili, A. H. Gandomi, S. Z. Mirjalili, S. Saremi, H. Faris, and S. M. Mirjalili, "Salp swarm algorithm: A bio-inspired optimizer for engineering design problems," *Adv. Eng. Softw.*, vol. 114, pp. 163–191, Dec. 2017.

[25] M. Premkumar and R. Sowmya, "An effective maximum power point tracker for partially shaded solar photovoltaic systems," *Energy Rep.*, vol. 5, pp. 1445–1462, Nov. 2019.

[26] M. Mao, L. Zhang, P. Duan, Q. Duan, and M. Yang, "Grid-connected modular PV-converter system with shuffled frog leaping algorithm based DMPPT controller," *Energy*, vol. 143, pp. 181–190, Jan. 2018.

[27] T. Sen, N. Pragallapati, V. Agarwal, and R. Kumar, "Global maximum power point tracking of PV arrays under partial shading conditions using a modified particle velocity-based PSO technique," *IET Renew Power Gener.*, vol. 12, no. 5, pp. 364–555, Apr. 2018.

[28] D. Pilakkat and S. Kanthalakshmi, "An improved P&O algorithm integrated with artificial bee colony for photovoltaic systems under partial shading conditions," *Sol. Energ.*, vol. 178, pp. 37–47, Jan. 2019.

[29] K. Sundareswaran, V. Vigneshkumar, P. Sankar, S. P. Simon, P. S. Rao Nayak, and S. Palani, "Development of an improved P&O algorithm assisted through a colony of foraging ants for MPPT in PV system," *IEEE Trans. Ind. Informat.*, vol. 12, no. 1, pp. 187–200, Feb. 2016.

[30] M. Kermadi, Z. Salam, J. Ahmed, and E. M. Berkouk, "An effective hybrid maximum power point tracker of photovoltaic arrays for complex partial shading conditions," *IEEE Trans. Ind. Electron.*, vol. 66, no. 9, pp. 6990–7000, Sep. 2019.

[31] S. Mohanty, B. Subudhi, and P. K. Ray, "A new MPPT design using grey wolf optimization technique for photovoltaic system under partial shading conditions," *IEEE Trans. Sustain. Energy*, vol. 7, no. 1, pp. 181–188, Jan. 2016.

[32] Y. Wan, M. Mao, L. Zhou, Q. Zhang, X. Xi, and C. Zheng, "A novel nature-inspired maximum power point tracking (MPPT) controller based on SSA-GWO algorithm for partially shaded photovoltaic systems," *Electronics*, vol. 8, no. 6, p. 680, Jun. 2019.

[33] S. Mirjalili, S. M. Mirjalili, and A. Lewis, "Grey wolf optimizer," *Adv. Eng. Softw.*, vol. 69, pp. 46–61, Mar. 2018.

[34] X. He, X.-S. Yang, M. Karamanoglu, and Y. Zhao, "Global convergence analysis of the flower pollination algorithm: A discrete-time Markov chain approach," *Procedia Comput. Sci.*, vol. 108, pp. 1354–1363, Apr. 2017.

[35] G. Xu and G. Yu, "On convergence analysis of particle swarm optimization algorithm," *J. Comput. Appl. Math.*, vol. 333, no. 1, pp. 65–73, May 2018.

[36] F. Davoodkhani, S. A. Nowdeh, A. Y. Abdelaziz, S. Mansoori, S. Nasri, and M. Alijani, "A new hybrid method based on gray wolf optimizer-crow search algorithm for maximum power point tracking of photovoltaic energy system," in *Modern Maximum Power Point Tracking Techniques for Photovoltaic Energy Systems* (Green Energy and Technology). Cham, Switzerland: Springer, Jul. 2019, pp. 421–438.

[37] F. S. Pai and P. S. Tseng, "An efficient GWO MPPT for a PV system using impedance information acceleration," *Int. J. Electron.*, vol. 106, no. 4, pp. 649–661, Apr. 2019.

[38] C. S. Kumar and S. R. Rao, "Enhanced grey wolf optimizer based MPPT algorithm of PV system under partial shaded condition," *Int. J. Renew. Energy Develop.*, vol. 6, no. 3, pp. 203–212, Oct. 2017.

LICHUANG CUI was born in Luohe, China, in 1996. He received the B.S. degree from the Liaoning University of Technology, Liaoning, China, in 2018. He is currently pursuing the M.S. degree in electrical engineering with Chongqing University, Chongqing, China. His current research interests include advanced control for renewable energy systems, power electronics, and artificial intelligence algorithms.

MINGXUAN MAO (Member, IEEE) was born in Luoyang, China, in 1988. He received the Ph.D. degree from Chongqing University, Chongqing, China, in 2017. From June 2016 to June 2017, he was a Visiting Scholar with the University of Leeds, Leeds, U.K., where he was involved in research on renewable energy systems and optimal control of power electronic converters. In 2018, he joined the State Key Laboratory of Transmission and Distribution Equipment and Power System Safety and New Technology, Chongqing University, where he is currently a Postdoctoral Research Fellow and a Lecturer. His current research interests include advanced control for renewable energy systems, power electronics, and artificial intelligence algorithms.

LIN ZHOU was born in Sichuan, China, in 1961. He received the Ph.D. degree in electrical engineering from the Department of Electrical Engineering, Chongqing University, Chongqing, China, in 2004, where he is currently a Professor with the State Key Laboratory of Transmission and Distribution Equipment and Power System Safety and New Technology. He is also involved in teaching and scientific research of power systems. His current research interests include the key technology of distributed generation and power quality control.

KE GUO was born in Guanghan, China, in 1973. He received the B.S. and M.S. degrees from the Department of Electrical Engineering, Chongqing University, Chongqing, China, in 1996 and 2008, respectively. He is currently with the State Key Laboratory of Transmission and Distribution Equipment and Power System Safety and New Technology, Chongqing University. He is also involved in teaching and scientific research of power electronic technology and power systems. His research interests include application of embedded systems and distributed generation.

QIANJIN ZHANG was born in Shandong, China, in 1992. He received the B.S. degree from Shandong Agricultural University, Shandong, China, in 2015. He is currently pursuing the Ph.D. degree with the Chongqing University, Chongqing, China. He is also involved in research on the modeling, control, and stability analysis of power electronics-based renewable systems.

● ● ●